PROCEEDINGS, 43rd Workshop on Geothermal Reservoir Engineering
Stanford University, Stanford, California, February 12-14, 2018
SGP-TR-213

Nano-/Microparticle Tracers for Evaluating Structures in Fractured Porous Media

Anna Suzuki[1†], Junzhe Cui[1], Yuran Zhang[2], Kewen Li[2], Roland N. Horne[2]

[1]Institute of Fluid Science, Tohoku University, 2-1-1 Katahira, Aoba-ku, Sendai, Miyagi, 980-8579, Japan

[2]Department of Energy Resources Engineering, Stanford University, 367 Panama Street, Stanford, CA, 94305, USA

[†]anna.suzuki@tohoku.ac.jp

Keywords: tracer test, fracture characterization, micro model, flow experiment

ABSTRACT

Nano- and microparticle tracers are expected to be used for evaluating structures in geological developments, however their transport behavior is not well characterized. This study investigated nanoparticle transport in a fractured medium through a microscope. A single fracture and rock matrix (grain and pore space) were fabricated on a silicon wafer, which is called a micromodel. Water and nanoparticles were injected into the micromodel, and the temporal change of particle concentration was measured by analyzing the scanning electronic mirror (SEM) images of the dried droplet. The response curve showed a peak at early time followed by a long tail, which suggests that some particles flowed through the fracture in the micromodel and others migrated through the matrix space. Tunable Resistive Pulse Sensing (TRPS) was also used to obtain temporal changes of the particle concentration. The larger particles were observed only at early time, while the smaller particles were detected over a wider range of time. This indicates that particles with different sizes transport through fractured media differently depending on the fracture structures and that the tracer response may be useful to evaluate the flow properties for each flow path.

1. INTRODUCTION

Understanding mechanisms of fluid flow in fractured porous media is essential for geoscientific research. Because the fluid flow in fractured rocks is controlled by complex fractures, the fracture structures need to be characterized. Tracer testing has been conducted to evaluate flow properties, such as connectivity, flow velocity, and dispersivity. However, spatial heterogeneities of fracture distributions cannot be obtained from the response of conventional solute tracers. Fluid with nano- and microsized particles have been investigated in several fields (e.g., medicine, optics, and electronics) (Taylor et al., 2013). Geological development also expects to use nano- and microparticles as tracers, which may provide more effective information for reservoir characterization and improve the efficiency of energy resources development (Burtman et al., 2015).

Nano- and microparticles embedding specific materials may provide new methodologies to estimate spatial heterogeneities of fracture distributions. Burtman et al. (2015) conducted the measurements of electrical conductivity of brine with nanoparticles (Fe_3O_4, Fe_2O_3, NiO, and Al_2O_3) and showed the possibility to observe significant difference of conductivity with nanoparticles in rocks. Angayarkanni and Philip (2014) showed a 4366 % increase in electrical conductivity for SiO_2 water-based nanofluids due to the effect of the double electric layer surrounding each particle and particle size effect. If we use highly conductive nanofluid for Electrical Resistivity Tomography (ERT), time histories of three-dimensional spatial distributions of tracer migration in fracture networks may be obtained.

A DNA (deoxyribonucleic acid)-based nanotracer can be produced by attaching synthetic DNA molecules to the surface of a silica nanoparticle seed and adding a protective outer silica layer. DNA protected by silica nanoparticles has been proven to withstand temperature as high as 200°C (Paunescu et al., 2013), which potentially makes it applicable to high temperature regions in geothermal fields. A DNA molecule is composed of four types of nucleotides, and the different arrangements of nucleotides that compose a long DNA double helix result in DNA molecules with almost infinite possible sequences. The infinite number of DNA sequences leads to an unlimited number of uniquely identifiable nanoparticle tracers which could be applied to multiple wells or thousands of flow paths for tagging purposes without ambiguity (Zhang et al., 2017).

The ability to control size and shape is also an advantage of using nano-/microparticles as tracers. Most geothermal reservoirs are thought to have fluid passing through fractures with apertures of a few nano- and micrometers. If particles with different sizes are injected, only particles smaller than the largest aperture in the flow path are able to pass. Thus, it can be estimated that the size of the observed largest particle is the minimum aperture in the flow path. Nishiyama and Yokoyama (2017) investigated pore sizes and flow properties in porous rocks and found that the narrowest pore throat diameter has an influence on the bulk flow velocity through the flow path. They introduced a critical pore radius corresponding to a radius of the largest sphere that can freely pass through the porous medium. We aim at using nano- and microparticle tracers to identify the minimum fracture aperture in a flow path, which is called the critical aperture, and to evaluate their flow characteristics.

A schematic of the proposed method using particle tracers to estimate critical apertures is shown in Figure 1. Particles with a wide range of particle sizes are injected into an injection well, and the temporal changes of the size distributions are observed at the production well. The tracer response curve for each particle size may be different. As shown in Figure 1, *path* 1, *path* 2, and *path* 3 have the critical aperture b_1, b_2, and b_3, respectively ($b_1 > b_2 > b_3$). Let us assume that adsorption/desorption and diffusion of particles do not occur and that clogged particles do not affect other particles' movements. Some interactions between particle and rock surfaces (van der Waals forces) are neglected. If particles are larger than b_1, they cannot pass through any of the paths. The upper tracer response curve in blue in Figure 1 is for the particles with size between b_2 and b_1. Particles with size between b_2 and b_1 migrate through *path* 1 but not through *path* 2 and *path*

3. The tracer response curve includes a single peak at t_i. The first peak is an indication of the tracers passing through *path* 1 with a critical aperture of b_1. Although other particles that ranges from b_3 to b_2 (green line) or smaller than b_3 (red line) were also detected at t_i, those are neglected. Next, only the particles with size smaller than b_3 (red line) shows the second peak at t_{ii},. The second peak is an indication of the tracers passing through the *path* 3 with a critical aperture of b_3. The particles with a size between b_3 and b_2 (green line) showed a third peak at t_{iii}, suggesting tracers passing through the *path* 2. We consider that the time when each peak appeared (i.e., t_i, t_{ii}, and t_{iii}) is the representative travel time of particles for each flow path. In this example, the travel time t_i is for the *path* 1, the travel time t_{ii} is for the *path* 2, and the travel time t_{iii} is for the *path* 2. The permeability can be estimated according to the cubic law by using estimated critical apertures. The flow velocity for each path can be obtained from the Darcy's law. Because the particles in the same flow path may have distinct velocity and travel time, it is possible to estimate the length of each actual flow path.

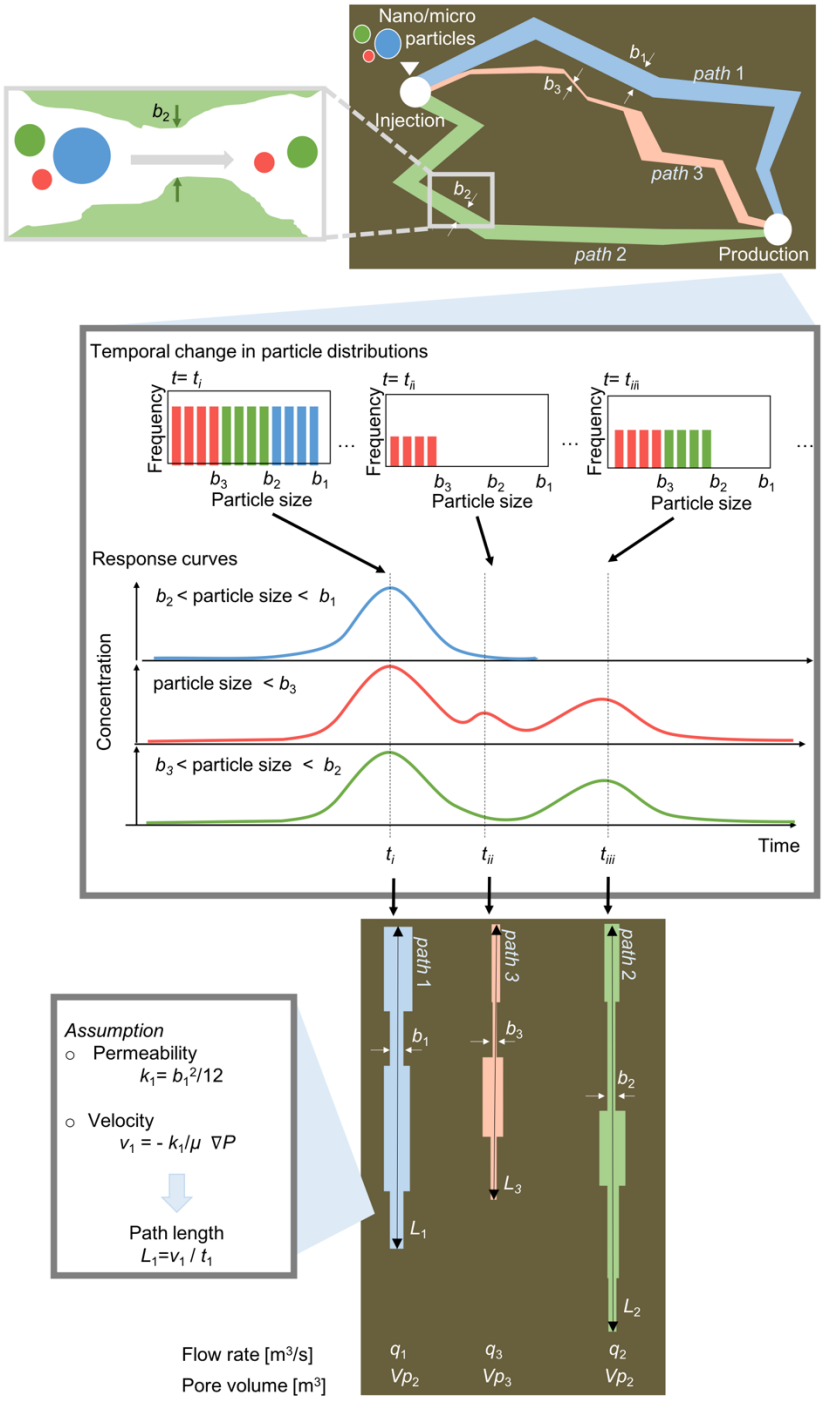

Figure 1: Schematic of estimating fracture aperture and lengths using nano/microparticles.

As mentioned, particle tracers embedded with specific material or fabricated with specific size may provide new methodologies to estimate spatial heterogeneities. The use of nanoparticles as tracers is expected to improve the effectiveness of subsurface evaluation, by allowing more accurate, more precise, and better controlled measurements from tracer responses. Some experimental investigations have been conducted to assess nanoparticle mobility in water-saturated glass-beads packs or sandpacks (e.g., Zhang et al., 2015). The transport of nano-/microparticles shows different behaviors from conventional solute tracers. However, the cause is not understood clearly yet. Recently, pore-scale flow has been studied in micromodels, which are composed of a transparent glass and networks of porous structures and provide direct observation of the internal processes at pore scale through a microscope (Keller and Auset, 2007). Alaskar et al. (2013) created a micromodel including a single fracture and matrix patterns (grain and pore spaces) obtained from real rocks. In this work, we aimed at developing a method to evaluate rock structures in fractured porous media. Particle transport in fractured porous media was visualized by using the micromodel. The tracer response curve was analyzed by SEM imaging and Tunable Resistive Pulse Sensing (TRPS). The effect of fracture structure and tracer properties on particle transport was investigated.

2. METHODOLOGY

2.1 Nanoparticles

We used 500 nm green fluorescent silica particles (Corpuscular Inc., New York, USA) in this study. The density of the particles was approximately 2.0 g/cm^3. The original concentration of the particles was 2.5mg/ml. The excitation and emission wavelengths were 480 nm and 530 nm, respectively. Figure 2 shows an image of nanoparticles obtained from a scanning electron microscope (SEM). 1µl of sample was dropped on a substrate and dried before the SEM observation. As shown in Figure 2, the diameter of all of the particles was approximately 500 nm. The particles were well-shaped.

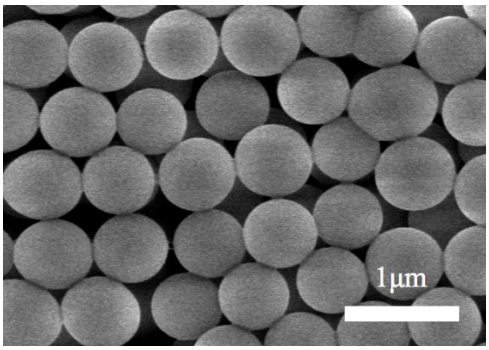

Figure 2: SEM image of nanoparticles.

The particle size was also measured by the qNano (Izon Science Inc.) using Tunable Resistive Pulse Sensing (TRPS) (Platt et al., 2012). A schematic of the TRPS system and an image of the qNano are shown in Figure 3. The qNano consists of a tunable pore sandwiched between the upper and lower fluid cells. At the beginning, the cells were filled with conductive liquid. A voltage was applied between two electrodes on the upper and lower cells, which controls the flow of electrical current through the tunable pore. When individual particles pass through the pore, they briefly increase the electrical resistance and create a resistive pulse, which is precisely proportional to particle volume. The measurement of particle size by the qNano is shown in Figure 4. The particle diameters were from 500 nm to 1500 nm, which is consistent with the observation of the SEM images.

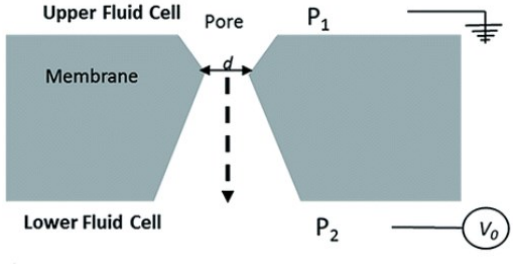

(a)

(b)

Figure 3: (a) System of Tunable Resistive Pulse Sensing (TRPS) and (b) image of qNano apparatus.

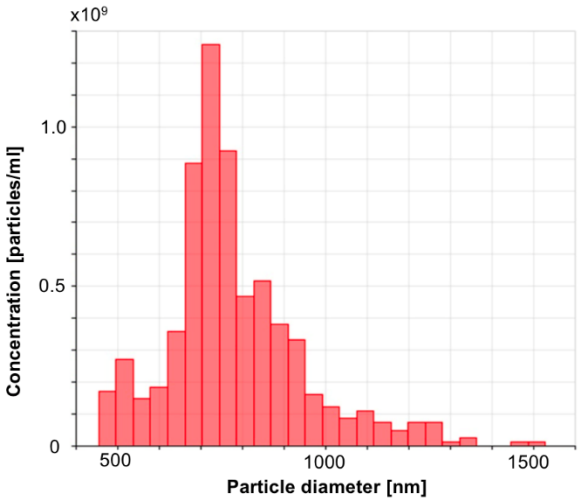

Figure 4: Frequency of silica nanoparticle diameters measured by TRPS.

The particles employed were negatively charged as specified by the manufacturer. The average zeta potential was -80.2 mV (standard deviation: 1.77 mV). The particles exhibited a high repulsive energy barrier above 1000 K_BT, which should render them free from aggregation and/or attachment to rock walls.

2.2 Micromodel

The micromodel used in this study was the same model as presented in Alaskar et al. (2013). The model was fabricated at the Stanford Nanofabrication Facility (SNF). The micromodel was made of 4-inch silicon wafers, K Prime, 4P <100> B S42565. A schematic of the micromodel is shown in Figure 5. The black parts in Figure 5 to be filled with water were dry-etched using an inductive charged plasma deep reactive ion etcher. The etched silicon wafer was covered with a transparent glass by anodic bonding. The glass had two holes, which were connected to tubing as the inlet and the outlet.

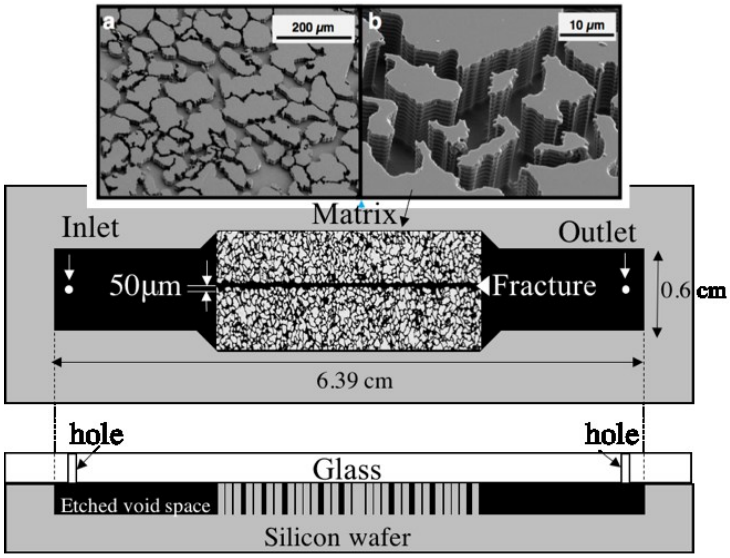

Figure 5: Schematic of the micromodel. The gray part is silicon wafer, and the black part is void spaces to be filled with water.

The model consisted of a single fracture of 50 μm aperture surrounded by matrix on both sides. The pore network in the matrix was designed by using a thin section of real sandstone. The average pore size in the micromodel was about 9.53 μm. The grain sizes of the micromodel ranged from 3.7 to 133.2 μm, and the average was 60.9 μm. The depth of the pores and/or fracture channel was 6.4 μm (± 0.7), measured by SEM. The porosity was calculated as the ratio of pore void area to the total area using image analysis, and was found to be 31.5%.

2.3 Flow Experiment

The micromodels were saturated by flowing CO_2 and pure water (Q-Millipore) until full saturation was achieved. Water was injected by 2 m water head difference at room temperature. Flow rate was 4.65×10^{-4} cm^3/min. 1:20 dilution of tracer of 0.5 ml was injected as a pulse at the inlet.

3. Results and Discussion

Water with nanoparticles was injected into the micromodel. The microscope could detect 500 nm nanoparticle movement. Figure 6 shows an image of the micromodel in the microscope during tracer injection test. Video was also recorded, which made it clear to see the particle movement. Fast flow was created in the fracture in the direction of flow, while some particles migrated to the pore spaces in the matrix. In the matrix, there were not only vertical flows from the fracture to the matrix but also horizontal flows between the inlet and the outlet. The patterns of pore space in the matrix give rise to complex nanoparticle transport behavior. More detailed analysis of nanoparticle movement will be done in further study (e.g., using Particle Image Velocimetry).

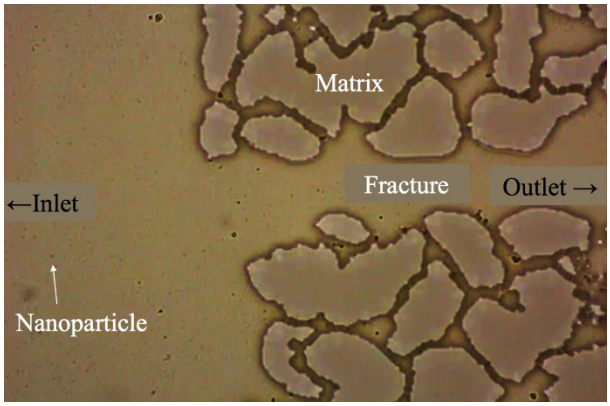

Figure 6: Image of the micromodel under microscope during flow experiment.

Tracer was collected in a tubing connected to the outlet at 46 points. For preliminary analysis, concentration was calculated based on the image data taken with the SEM. Five droplets obtained at 6.7h, 13.4h, 20.2h, 26.9h, and 33.6h after the onset of the particle injection were used. The SEM images of the five droplets are shown in Figure 7. The concentration was calculated as the ratio of area of the particles to the total area where liquid would have existed in the SEM images, as shown in Figure 8(a). The temporal change of the concentration is plotted in Figure 8(b). High concentration was found at 13.4 h. A long tail was observed at late time. Some non-nanoparticle chunks were observed in the image at 26.9h. Because they were probably contaminant, the concentration at 26.9h is of low reliability. If the concentration at 26.9h is an outlier, the tracer response shows a long tail, as plotted in the dashed line in Figure 8(b). From direct observation under the microscope, some particles were seen to migrate into the matrix. They might have detoured through the pore space in the matrix leading to the retardation in the tracer response curve.

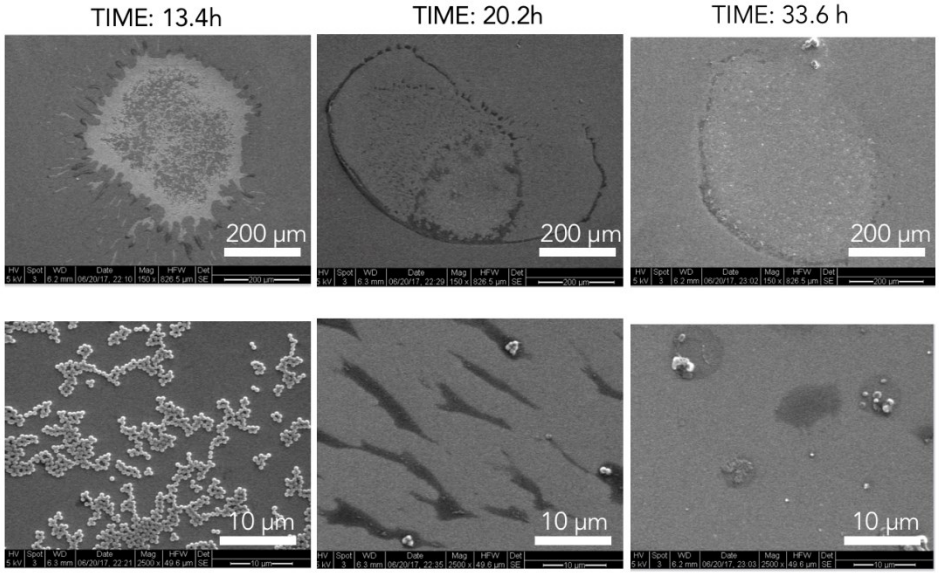

Figure 7: SEM images of droplet obtained at 13.4h, 20.2h, and 33.6h after injection.

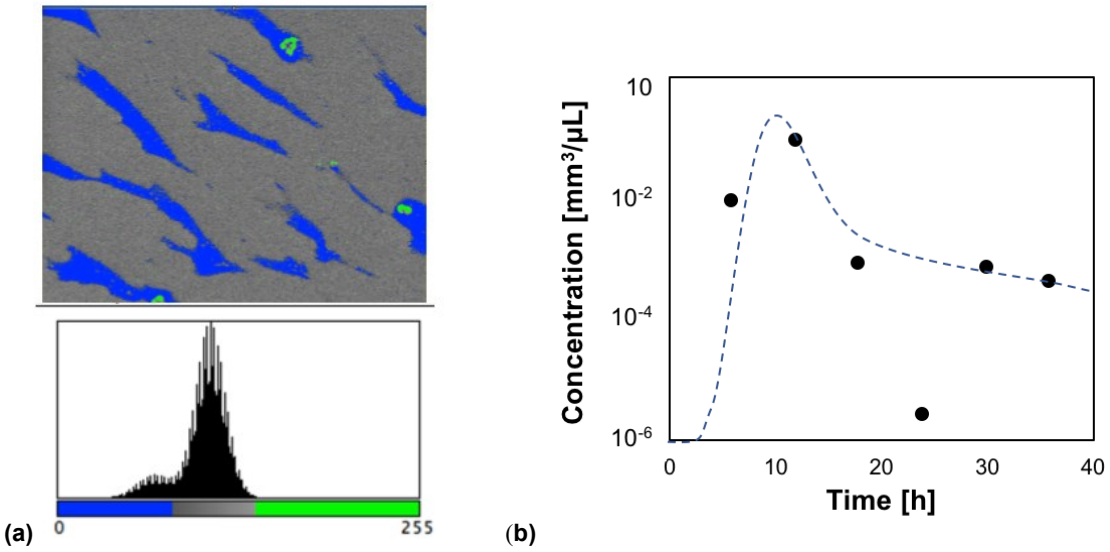

Figure 8: Calculation of particle concentration. (a) Image analysis from SEM images. (b) Concentration of particles in droplets.

Particle concentrations were also measured by TRPS. The TRPS counts the number of particles in liquid while measuring the size of the particles. Figure 9 shows the concentration of particle diameters in the droplet obtained at the outlet 2 hours after the onset of the injection. The particle diameter had a wide range between 400 nm and 2400 nm. Here, as shown in Figure 4, the maximum particle diameter before the injection was 1500 nm. However, the maximum particle diameter measured after flowing in the micromodel was 2300 nm, which was larger than that of the injected particles. This suggests that some particles may have aggregated or contaminated by attachment. 46 samples were collected at the outlet over time. The total number of particles obtained from each sample are plotted in Figure 10. Although SEM image analysis shows higher concentration around 14.4 hours after the injection, the concentration obtained from TRPS does not include any clear peak.

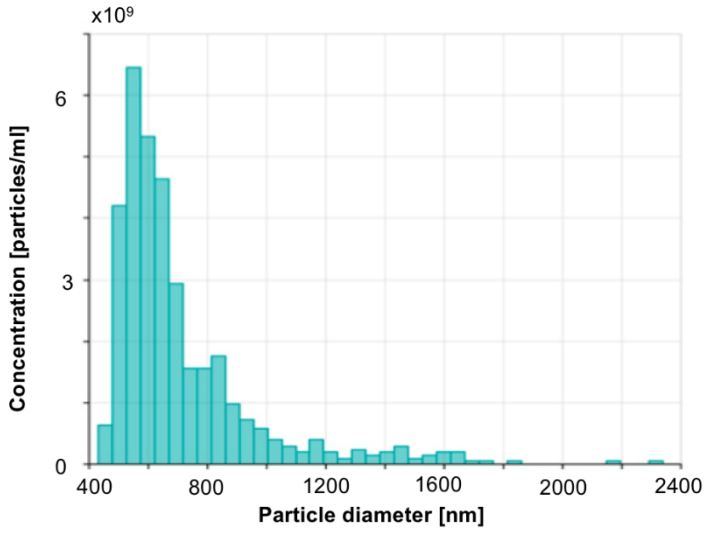

Figure 9: Concentration of nanoparticles in droplet obtained at outlet 2 h after injection.

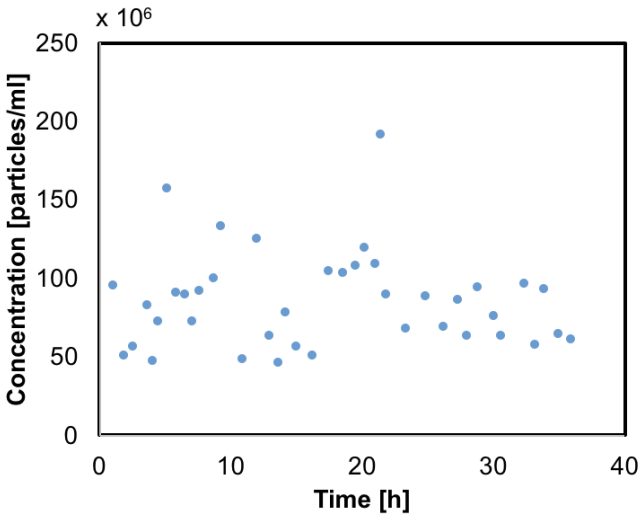

Figure 10: Concentration of nanoparticles at the outlet of the micromodel.

Thanks to the TRPS, particle size distributions at each time point can be obtained. We can divide the particle distributions into two groups by a certain threshold. The threshold is defined as a value below which significant differences can be observed in the concentration curves. In this study, the threshold was set to be 1700 nm. The temporal changes of the particle concentration with diameter larger or smaller than 1700 nm are shown in Figure 11(a) and (b), respectively. The response curve for the particles with diameter larger than 1700 nm had a peak around 14 hours after the injection and no concentration was detected at the late time. This result suggests that the particles larger than 1700 nm migrated in a fast flow path. The larger particles were able to pass through the fast flow path only. The fracture in the middle of the micromodel can be thought as the fast flow path. On the other hand, a clear peak was not observed for smaller particle concentration, and similar concentrations were observed throughout the flow experiment for the smaller particles. If we assume that the effect of particle size on flow velocity is negligible, smaller and larger particles appearing around 14 hours after the injection flowed through the fracture. Because microscopy suggested that some particles migrated in the pore space in the micromodel, the particles appearing at later time should not only migrate in the fracture but also transported through the pore space.

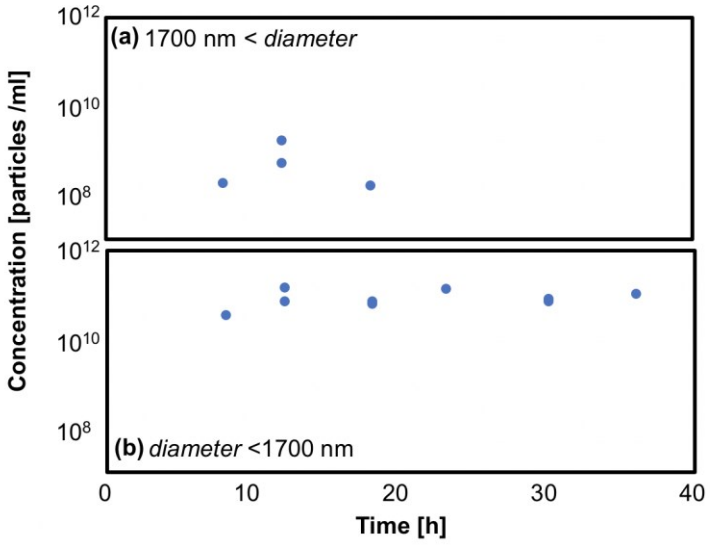

Figure 11: Concentration of nanoparticles for particles (a) larger and (b) smaller than 1700 nm, respectively.

Figure 12 shows the frequency of pore throat diameters in the pore space of the micromodel. The range of the pore throat diameter was from 10 nm to 40 µm. Although the pore throat diameter of 2 µm was the most frequent, there were also a few occurrences of pore throats with a diameter around 1700 nm. As mentioned in the Introduction section, the particle size may be used to estimate critical aperture (minimum fracture aperture) in the flow path. Our result of tracer response suggests that the smallest fracture aperture in the flow path is 1700 nm. This indicates that the analysis of particle responses may be useful in estimating fracture and rock structures.

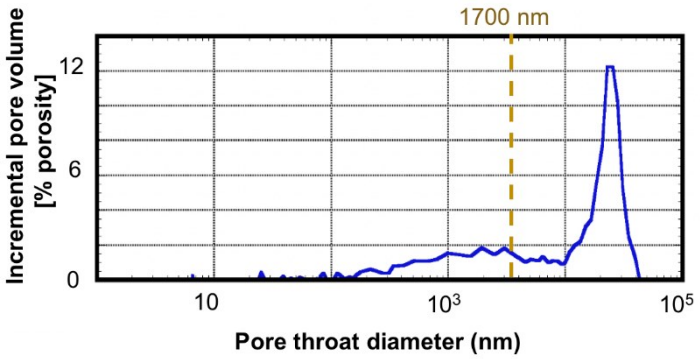

Figure 12: Frequency of pore throat diameter in pore space in micromodel.

This study used particles in the range between 500 nm and 1500 nm to confirm whether or not the particles can pass through the porous medium. In the next step, particles with a wider size distribution (e.g., 50 nm – 50 μm) will be used. The fracture aperture in the micromodel will also vary. Further experiments would provide more obvious relationships between particle sizes fracture structures. Although we assumed particle size does not affect flow speed, several studies reported that particle properties (e.g., size, materials, shape) affect the flow properties. We will investigate whether the dependence of particle properties on flow can be neglected in our scale by direct observation of the microscope.

4. CONCLUDING REMARKS

Nano- and microparticles are expected to have several functionalities. Our study shows that evaluation of particle size distributions may provide estimation on minimum fracture apertures in the flow path. Fluid flow experiments using micromodels will clarify mechanisms of particle transport in fractured and porous media, which will help us analyze tracer response curve more thoroughly.

ACKNOWLEDGEMENTS

Many thanks go to Dr. Mohamad Alaskar who let us use his micromodels at Stanford University. This work was supported by the Japan Society for the Promotion of Science, under JSPS KAKENHI Grant Number 717H049760, whose support is gratefully acknowledged.

REFERENCES

Alaskar, M., Li, K., and Horne, R. N.: Influence of particle size on its transport in discrete fractures: pore-scale visualization using micromodel, *Proceedings*, 38th Workshop on Geothermal Reservoir Engineering, Stanford University, Stanford, CA (2013).

Angayarkanni, S.A., and Philip, J.: Effect of nanoparticles aggregation on thermal and electrical conductivities of nanofluids, *Journal of Nanofluids*, **3**(1), (2014), 17-25, doi:10.1166/jon.2014.1083.

Burtman, V., Endo, M., Marsala, A., and Zhdanov, M.S. :Feasibility study of application of nanoparticles in complex resistivity (CR) reservoir monitoring, *SEG Technical Program Expanded Abstracts*, (2015), 963-967, doi:10.1190/segam2015-5868400.1.

Keller, A. A., Auset, M.: A review of visualization techniques of biocolloid transport processes at the pore scale under saturated and unsaturated conditions. *Advanced Water Resources*, **30**, (2007),1392-1407, doi:10.1016/j.advwatres.2006.05.013.

Nishiyama, N., and T. Yokoyama (2017), Permeability of porous media: Role of the critical pore size, *Journal of Geophysical Research: Solid Earth*, **122**, (2017) 6955–6971, doi:10.1002/2016JB013793.

Paunescu, D., Puddu, M., Soellner, J.O.B., Stoessel, P.R., and Grass, R.N. :Reversible DNA encapsulation in silica to produce ROS-resistant and heat-resistant synthetic DNA "fossils". *Nature Protocols*, **8**(12), (2013), 2440-2448, doi:10.1038/nprot.2013.154.

Taylor, R., Coulombe, S., Otanicar, T., Phelan, P., Gunawan, A., Lv, W., Rosengarten, G., Prasher, R., and Tyagi, H.: Small particles, big impacts: A review of the diverse applications of nanofluids. *Journal of Applied Physics*, **113**(1), (2013), doi:10.1063/1.4754271.

Zhang, T., Murphy, M.J., Yu, H., Bagaria, H.G., Yoon, K.Y., Neilson, B.M., Bielawski, C.W., Johnston, K.P., Huh, C., and Bryant, S.L. :Investigation of nanoparticle adsorption during transport in porous media. SPE Journal, (2015). 1-11, doi:10.2118/166346-PA.

Zhang, Y., Zeng, Z., Li, K., and Horne, R.N. :DNA Barcoding for fractured reservoir analysis – an initial investigation, *Proceedings*, 42th Workshop on Geothermal Reservoir Engineering, Stanford University, Stanford, CA (2017).